



Contents lists available at ScienceDirect

International Journal of Applied Earth Observation and Geoinformation

journal homepage: www.elsevier.com/locate/jag



Enhanced change detection index for disaster response, recovery assessment and monitoring of accessibility and open spaces (camp sites)



Dilkushi A. de Alwis Pitts*, Emily So

Department of Architecture, University of Cambridge, United Kingdom

1

2

3

4

Enhanced Change Detection Index for Disaster Response, Recovery Assessment and Monitoring of Accessibility and Open Spaces (Camp Sites)

6

7

Authors

8

9

Dilkushi A. de Alwis Pitts^a, Emily So^a

10

11

^aDepartment of Architecture, University of Cambridge, United Kingdom

12

13

email: kad49@cam.ac.uk

14

15

Abstract The availability of Very High Resolution (VHR) optical sensors and a growing image archive that is frequently updated, allows the use of change detection in post-disaster recovery and monitoring for robust and rapid results. The proposed semi-automated GIS object-based method uses readily available pre-disaster GIS data and adds existing knowledge into the processing to enhance change detection. It also allows targeting specific types of changes pertaining to similar man-made objects. This change detection method is based on pre/post normalized index, gradient of intensity, texture and edge similarity filters within the object and a set of training data. Once the change is quantified, based on training data, the method can be used automatically to detect change in order to observe recovery over time in large areas. Analysis over time can also contribute to obtaining a full

16

17

18

19

20

21

22

23

24 picture of the recovery and development after disaster, thereby giving managers a better understanding
25 of productive management practices.

26

27 **Keywords: Change Detection, Remote Sensing, Disaster Response and Recovery, Roads,**
28 **Open Spaces**

29

30 **1. Introduction**

31 Rapid and robust impact assessment of poorly-accessible affected areas is essential for initiating
32 effective emergency response actions following disasters (Dell'Acqua et al. 2009), especially in
33 highly populated urban areas (Vu and Ban 2010). Information pertaining to accessibility is critical in
34 order to organize medical help and evacuation as well as aiding in both early- and long-term recovery
35 evaluation (Joyce et al. 2013). In addition, identifying the location and sizes of open spaces is
36 important in the early phases of emergency response. This information allows emergency managers to
37 select the best plots for camps. These campsites also require monitoring and evaluation during in
38 early-recovery phase to understand the population's re-housing.

39 Information on damage caused by an event can be derived quickly from suitable very high-resolution
40 (VHR) satellite imagery (Walter, 2004) by comparing data from a chosen reference before the event
41 (pre-event) to imagery acquired shortly after the event (post-event). The availability of pre- and post-
42 event data opens the possibility for gathering impact assessment data using change detection in
43 complex environments such as urban areas. Change detection from high spatial-resolution images
44 such as IKONOS and QuickBird is even more challenging, especially in complex environments
45 characterised by small objects such as houses, individual trees and roads, and by shadows (Pagot et
46 al., 2008).

47 In general, change detection techniques can be grouped into two types: pixel-based and object-based
48 (Blaschke 2010, Chen et al., 2012). Pixel-based change detection analysis refers to using a change
49 detection algorithm to compare the multi-temporal images pixel-by-pixel while object-based change
50 detection analysis refers to using a change detection algorithm to compare multi-temporal images
51 object-by-object. However, the definition of pixel-based and object-based change detection is not
52 absolute. The most basic feature of object-based approaches is to segment the image and regard the
53 objects as the basic unit of operation, rather than the pixel-based approach, which regards a single
54 pixel as the basic unit (Dai, et al., 1998).

55 Object-based methods have the potential to provide more accurate results than traditional pixel-based
56 methods (Al-Khudhairy et al. 2005), but choosing the object feature is not straightforward because the

57 high information content of VHR images requires an accurate definition of the object. Thus the object
58 detection step causes most of the error (Michaelsen et al. 2006).

59 Most object-based algorithms concentrate on detecting objects such as rectangular buildings (Lin et
60 al. 1998) or parallel lines for detecting roads. This search is complex and rarely accurate, especially
61 after disasters. As noted in the related literature, road extraction has been achieved in single or
62 multiple operations such as image segmentation (Yang and Wang 2007, Singh et al. 2014),
63 classification (Mohammadzadeh et al. 2008), using morphological operations (Mena and Malpica
64 2005, Al-Khudhairy et al. 2005) and merging relevant road segments (Akçay and Aksoy 2008,
65 Mohammadzadeh, 2009). Hough transform and edge detection have also been used to detect linear
66 parallel segments with constant width (Talib and Ramli 2015), snakes (Butenuth and Heipke 2010)
67 (contour-based object outlines) and matching road templates to obtain networks (Touya 2010).
68 Hiremath et al., 2010 have used a sequence of filtering followed by segmentation, grouping and
69 optimization on VHR images to identify open spaces in complex urban environments.

70 Many current change-detection mechanisms do not make effective use of available pre-disaster data
71 and existing knowledge. Hence using pre-disaster GIS objects such as roads, open spaces, bridges etc.
72 as indicators allows targeting the search for specific changes to these areas within the objects of
73 interest. The proposed indicator-specific method uses readily available pre-disaster GIS data and
74 existing knowledge to enhance the detection of change while offering the possibility to target specific
75 types of changes pertaining to similar man-made objects.

76 The GIS object-based method discussed here is based on a pre/post normalized index, gradient,
77 texture, and edge similarity filters within the object and an existing set of training data. The proposed
78 semi-automated method is evaluated with QuickBird, Geoeye 1, and Worldview 2 datasets for
79 abrupt changes soon after a disaster. The method could also be automated to monitor progressive
80 changes months after a disaster.

81

82 **2. Method**

83 **2.1. Case Study Sites**

84 **2.1.1. Van, Turkey**

85 The Van earthquake was a destructive M7.1 earthquake that struck the city of Van in eastern Turkey
86 on Sunday, 23 October 2011 at 13:41 local time. Based on the reports at least 534 people were killed,
87 2,300 injured and 14,618 buildings and homes destroyed or damaged in the Ercis-Tabanlı-Van area
88 (Earthquake.usgs.gov 2015). As a part of the SENSUM (European Commission under FP7 (Seventh
89 Framework Programme): SENSUM: Framework to Integrate Space-based and in-situ sENSing for

90 dynamic vUlnerability and recovery Monitoring, 312972) project, the Van earthquake was selected
 91 for study because it was one of the most recent destructive, vast earthquakes for which imagery was
 92 available and suitable for a data-poor country for which remotely sensed tools were well suited.

93

94 **Table 1 Satellite Data for Van, Turkey**

Imagery	Acquisition Date
Pre- disaster (WV02)	06th May 2011 - 5 months before earthquake
Post disaster 1 (Geoeye-1)	12th Jan 2012 - 2.5 months after earthquake
Post disaster 2 (Geoeye-1)	22nd Feb 2012 - 3 months after earthquake
Post disaster 3(WV02)	05th June 2013 - 1 year and 7 months after earthquake

95 The WV02 (WorldView-2) sensor provides a high-resolution Panchromatic band and 8 multispectral bands: 4
 96 standard colors – (red(630 -690 nm), green (510 - 580 nm), blue (450 - 510 nm), and near-infrared 1(770 - 895
 97 nm) –and 4 new bands (coastal, yellow, red edge, and near-infrared 2). For this study we used only 4 spectral
 98 bands out of the 8 bands, omitting 4 new bands. The resolution of the Panchromatic (nominal at nadir) is 0.46
 99 m and multispectral (nominal at nadir) is 1.85 m. The Geoeye-1 has a Panchromatic band (450 - 800 nm) and 4
 100 multispectral bands, blue (450 - 510 nm), green (510 - 580 nm), red (655 - 690 nm) and near infrared (780 - 920
 101 nm). The resolution of the Panchromatic (nominal at nadir) is 0.41 m and multispectral (nominal at nadir) is
 102 1.65 m.

103 **2.1.2. Muzaffarabad, Pakistan**

104 The Kashmir earthquake was a destructive 7.6 Mw earthquake that struck the northwest region of
 105 Pakistan, near the city of Muzaffarabad, on 8 October 2005 at 08:52 local time (USGS, 2015).

106 The Muzaffarabad area was selected as a study site of the ReBuilDD (Remote sensing for Built
 107 environment Disaster and Development) (Brown et al.2012) project because it was a major earthquake
 108 with severe damage. The timing, the extent of the disaster and the fact that very little ground based
 109 data existed, made it a well suited as a case study of remotely sensed data.

110 **Table 2 Imagery and Data Acquisition dates for Muzaffarabad, Pakistan**

Imagery	Acquisition Date
Pre-disaster (QuickBird)*	13th August 2004 – 14 months before earthquake

Post disaster 1 (QuickBird)*	22nd October 2005 – 2 weeks after earthquake
Post disaster 2 (QuickBird)*	13th June 2006 – 8 months after earthquake

111 *QuickBird-2 imagery contained five bands namely Blue (450 - 520 nm), Green (520 - 600 nm), Red (630 - 690
 112 nm), NIR (760 - 900 nm), and PAN (760 - 850 nm). The spectral bands have a resolution of 2.44 m and the
 113 PAN band has a pixel resolution of 0.61 m nominal at nadir.

114
 115

116 **2.2. Data Acquisition and Data Preparation**

117 The process of initial data preparation for the proposed change detection method is shown in Figure 1.
 118 The following paragraphs explain the data preparation in detail.

119 **OpenStreetMap data:** The data pertaining to the road layer was downloaded directly from the
 120 OpenStreetMap (OSM) archive (GEOFABRIK (Download.geofabrik.de)). In the case of
 121 Muzzaffarabad, the street layers for the primary and secondary roads were manually digitised from
 122 the QuickBird VHR images using QGIS since the OSM data were incomplete.

123 **Satellite Images:** For the case study of Van, four satellite images were acquired from 2011 to 2013
 124 (Table 1). For the case study of Muzzaffarabad, three satellite images were acquired from 2004 to
 125 2006 (Table 2).

126 **Geo-rectifying the pre-disaster image:** All the satellite data were co-registered to the road layers
 127 obtained from OSM to ensure the best alignment (accuracy <1.47m). The pre-disaster IR R,G bands
 128 were first PAN-sharpened (using QGIS OTB (OrfeoToolBox) Processing toolbox) and then co-
 129 registered to the reference vector layer such as a road layer (See Figure 1).

130 **Geo-rectifying the post-disaster image:** The PAN-sharpened post-disaster image was geo-rectified
 131 using buildings, roads, and junctions identified in both the pre and post images and used as ground
 132 control points.

133

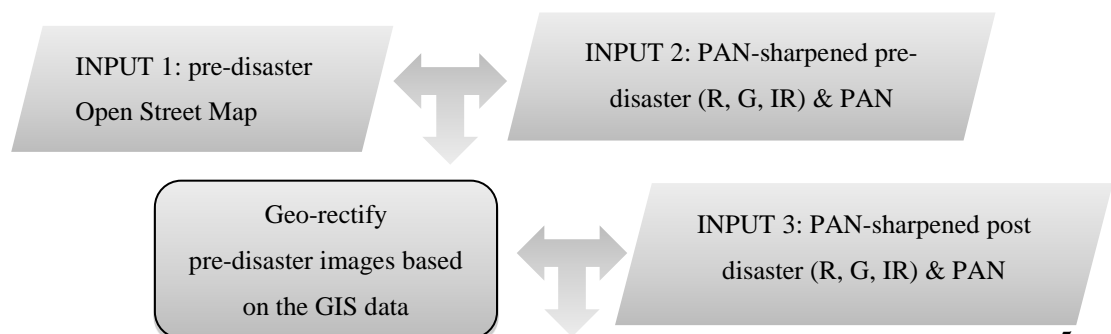
134

135

136

137

138



139
140
141
142
143
144
145
146
147
148
149

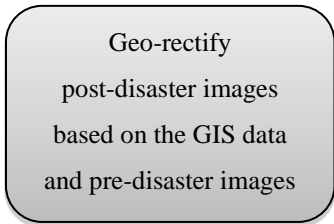
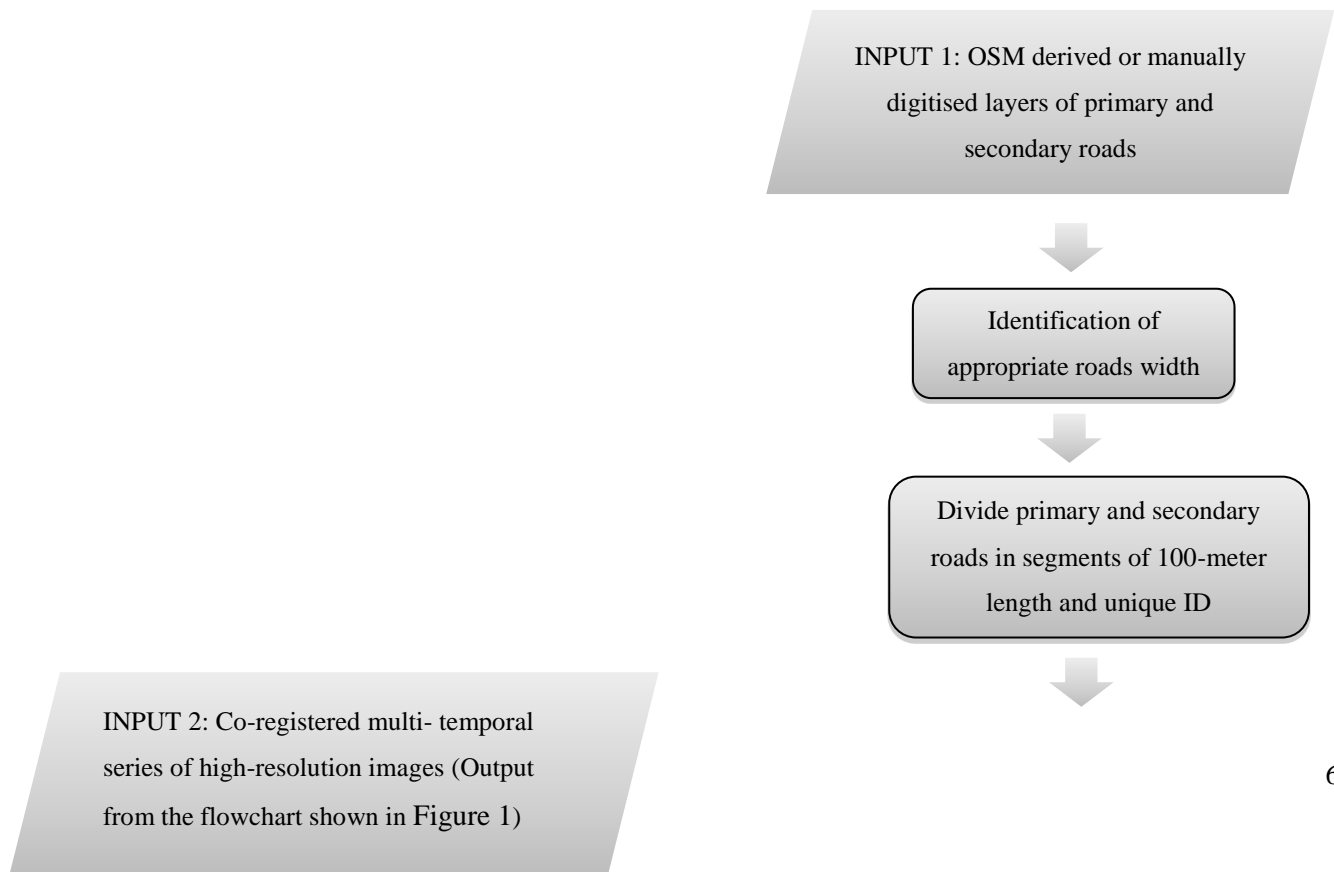


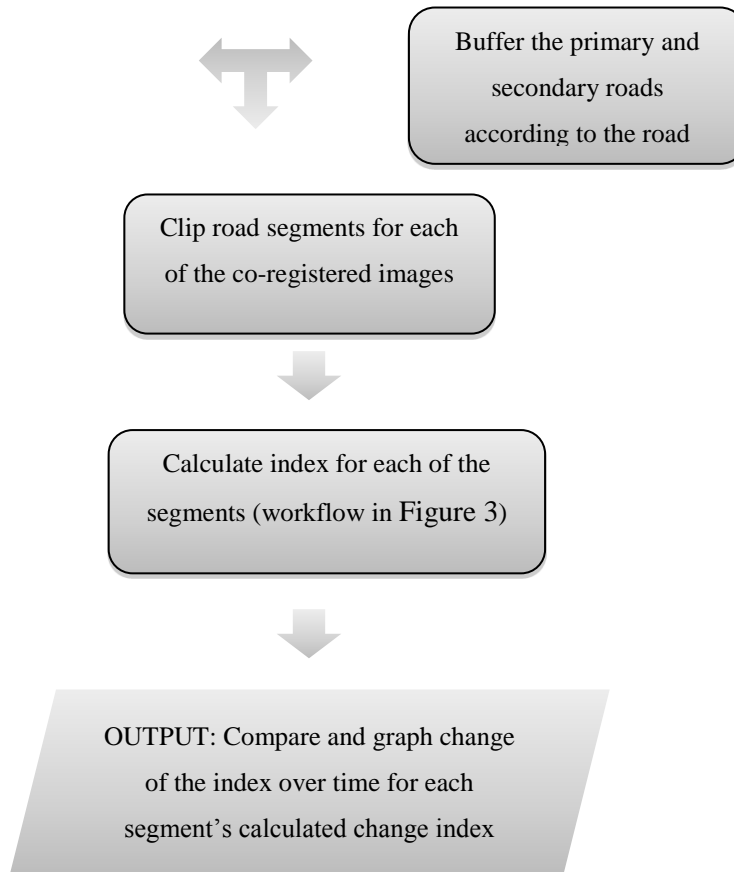
Figure 1 Data preparation workflow: Pre-disaster images are PAN-sharpened and geo-rectified to the Open Street Map and then the PAN-sharpened post-disaster images are geo-rectified to the pre-disaster images.

2.3. Accessibility: Building and Buffering Road Data

151 Before using the road layer in the accessibility workflow Figure 2, the road polylines were merged
152 and then split into 100-meter long segments. From visual inspection for Van, it was decided to apply a
153 6-meter buffer and a 4-meter buffer to represent primary and secondary roads respectively. For
154 Muzzaffarabad a buffer distance of 4 meters and 2 meters for primary and secondary roads was
155 identified. As seen in workflow Figure 2, each of the 100m segments was buffered and then clipped
156 for the complete time series, thus creating the multi-temporal set of raster road segments, which are
157 the input of the change detection index shown in Figure 3.

158





159 **Figure 2: The workflow for accessibility showing how the roads (GIS layers) are buffered and used to clip the pre-**
 160 **and post-images and prepare to calculate the Enhanced Change Detection Index**

161 **2.3.1. Pre-Post Normalized Difference of the Satellite data**

162 As per workflow in Figure 3 the pre-post normalized difference between the PAN-sharpened, geo-
 163 referenced bands (R, G, IR) and PAN bands is calculated using Equation 1 for each road segment.
 164 The pre-post normalized difference removes changes in reflectance due to acquisition times within the
 165 day. The normalized ratio in the denominator of Equation 1 helps to compensate for differences both
 166 in illumination within an image due to slope and aspect, and differences between images due to time
 167 of day or season when the images were acquired. Taking the square root is intended to correct values
 168 approximate a Poisson distribution and introduce a normal distribution, producing a linear
 169 measurement scale. Adding a constant of 0.5 to all pre-post normalized values does not always
 170 eliminate all negative values, but it leaves fewer of them.

171
$$\frac{\frac{POST-PRE}{POST+PRE+0.5}}{|\frac{POST-PRE}{POST+PRE+0.5}|} \cdot \sqrt{|\frac{POST-PRE}{POST+PRE} + 0.5|}$$
 Equation 1

172 **2.3.2. Enhanced Change Detection Index for Roads**

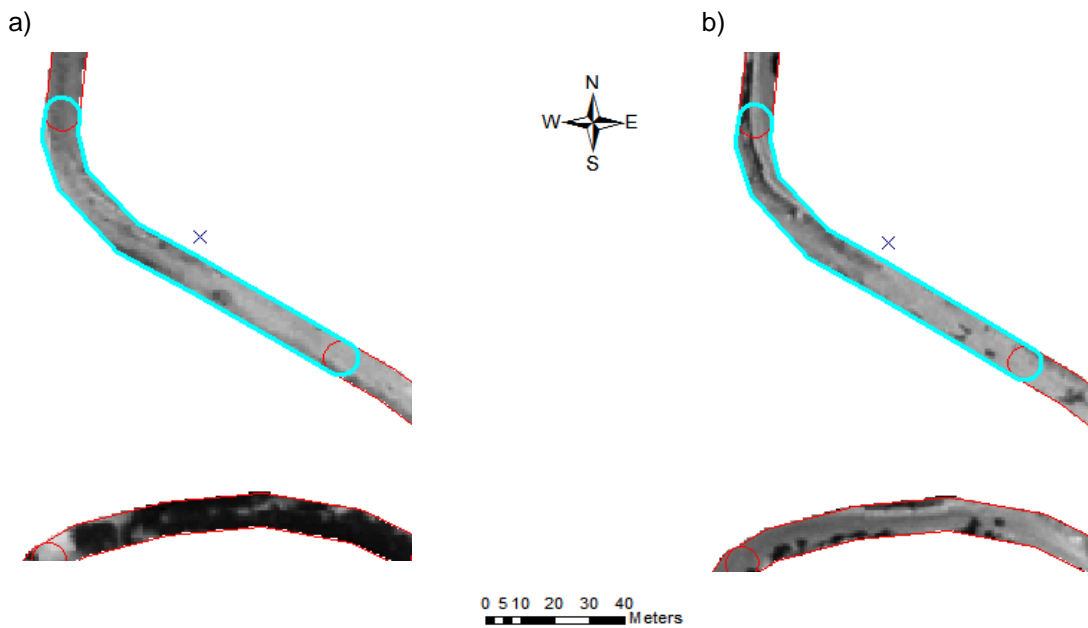
173 As shown in Figure 3 each normalized difference of PAN and PAN-sharpened (IR, R, G) bands for
 174 each road segment was subjected to Vigna edge detection in QGIS (QGIS Development Team,

175 2015) and texture using GDAL's (QGIS) roughness parameter. Edges and texture filters of the pre-
176 post normalized images were used to capture object specific changes in edges. Next the gradient is
177 calculated for each object in pre- and post-images PAN sharpened bands (R, G, IR) and PAN bands
178 and then normalized (for each band) using Equation 1. The change of edges, texture and gradient
179 parameters are calculated within each of the objects as per the flowchart in Figure 3 (accessibility).
180 This creates 12 change-related parameters (4 pertaining to edges, 4 to texture, and 4 to the gradient)
181 for each object in regard to accessibility (road segments).

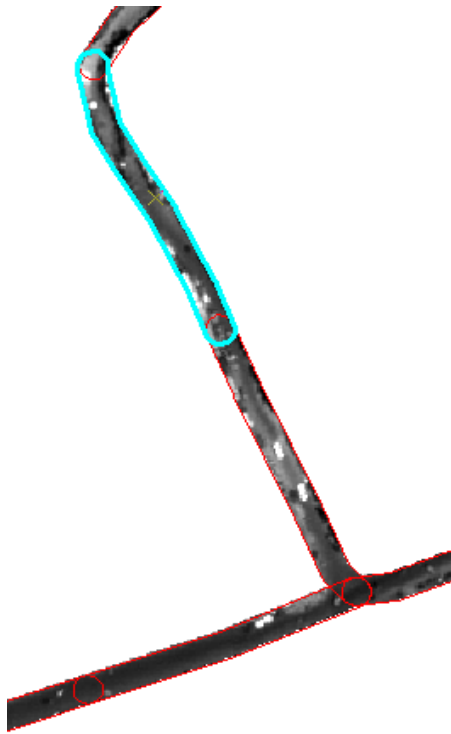
182 2.3.3. Visual Index (Training Data) for Road Segments

183

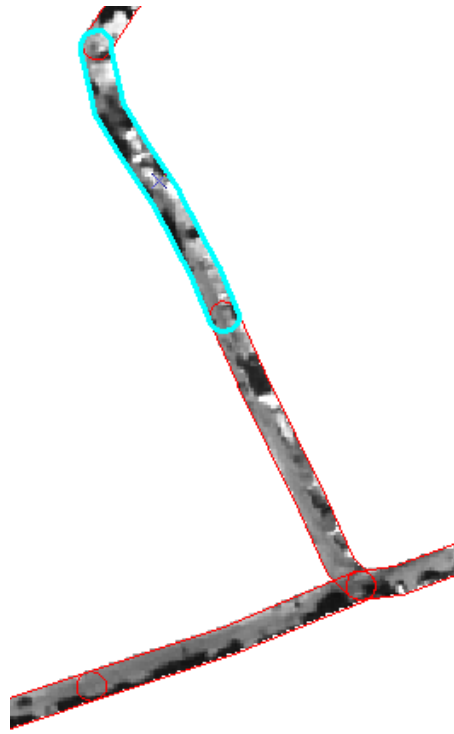
184 A visual index (VI) is developed by comparing the pre and post images visually in a way that is
185 analogous to a linear visual scale for change. This VI, in the range between 0 and 10 documents the
186 changes as perceived by a human. As shown in



c)



d)



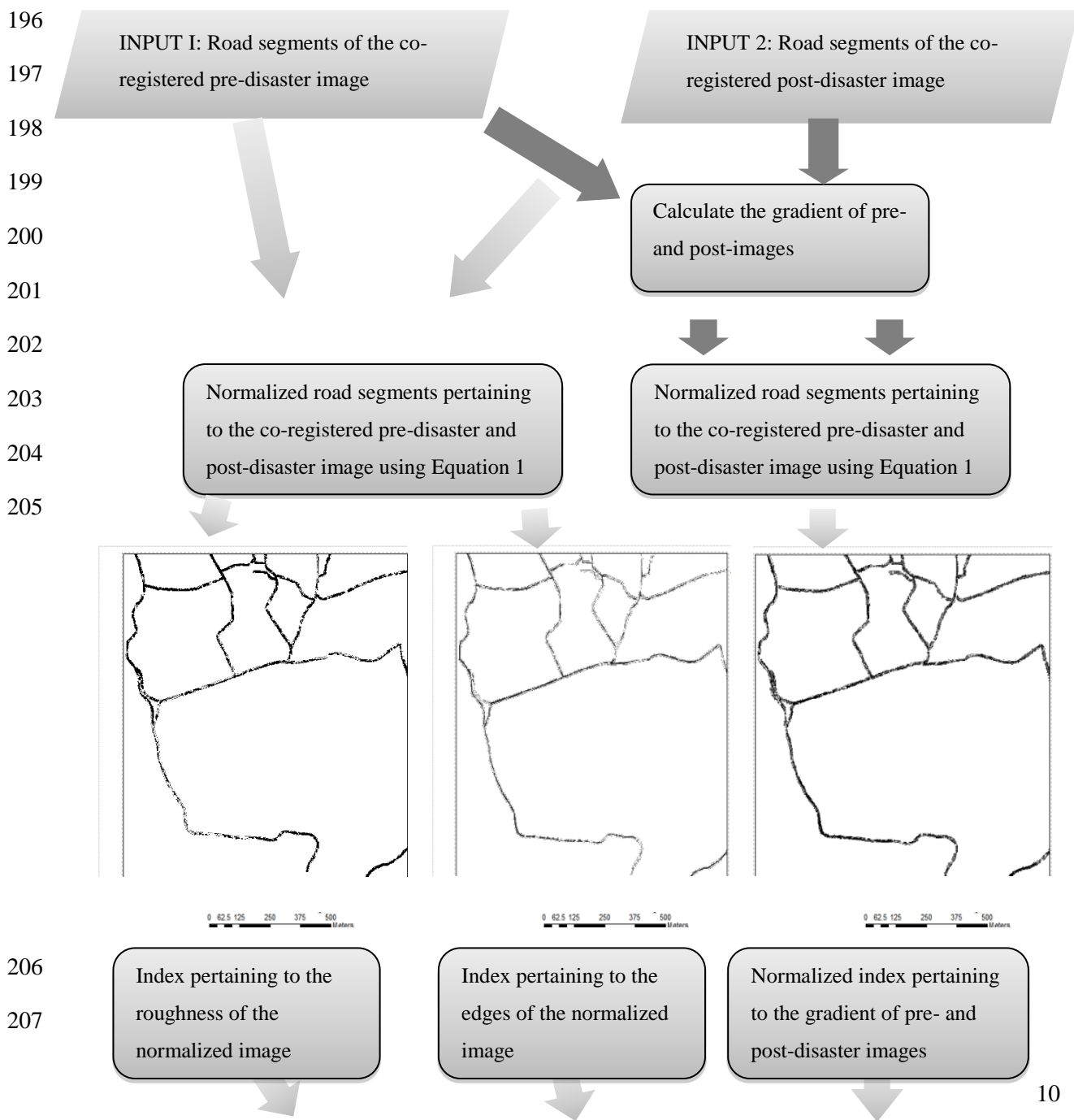
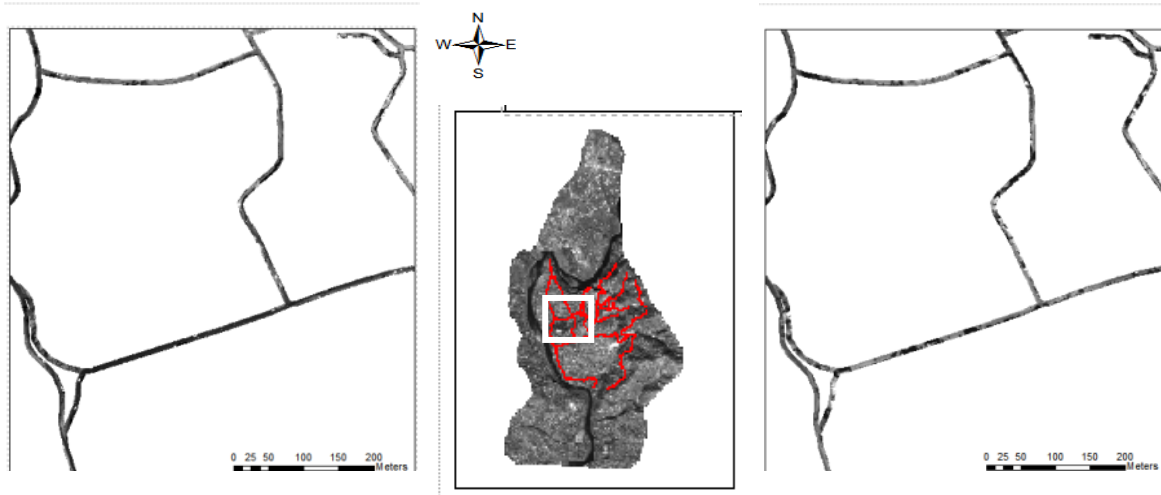
187 Figure 4, pre and post images of road segments (objects) of about 1/10 of the total road segments were
188 used visually to determine the VI. The segments that had mild changes were assigned a small VI
189 (close to 0, Figure 4 a) and b)) and the segments that showed large changes were assigned large VI
190 values (close to 10, Figure 4 c) and d)).

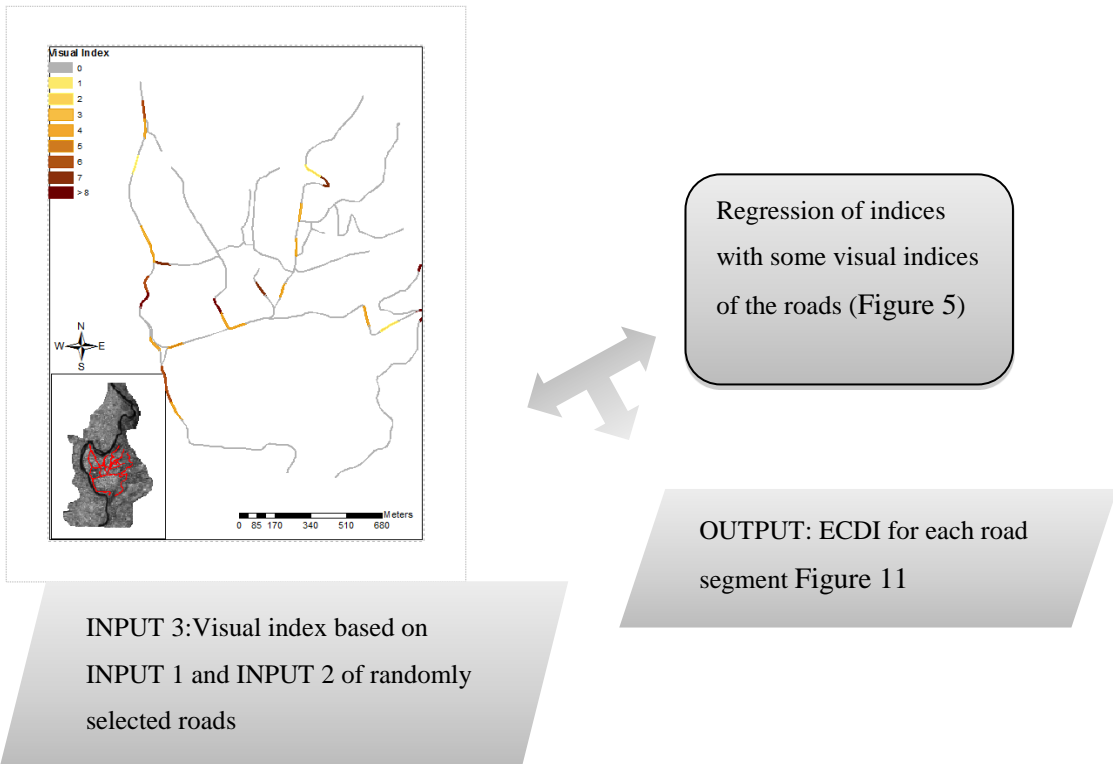
191 Then as seen in Figure 3, this visual index was used as a training set and regressed against the derived
192 values of pre-post normalized gradient, edges, and roughness of each road segment.

193

194

195





209

210

211

212

213

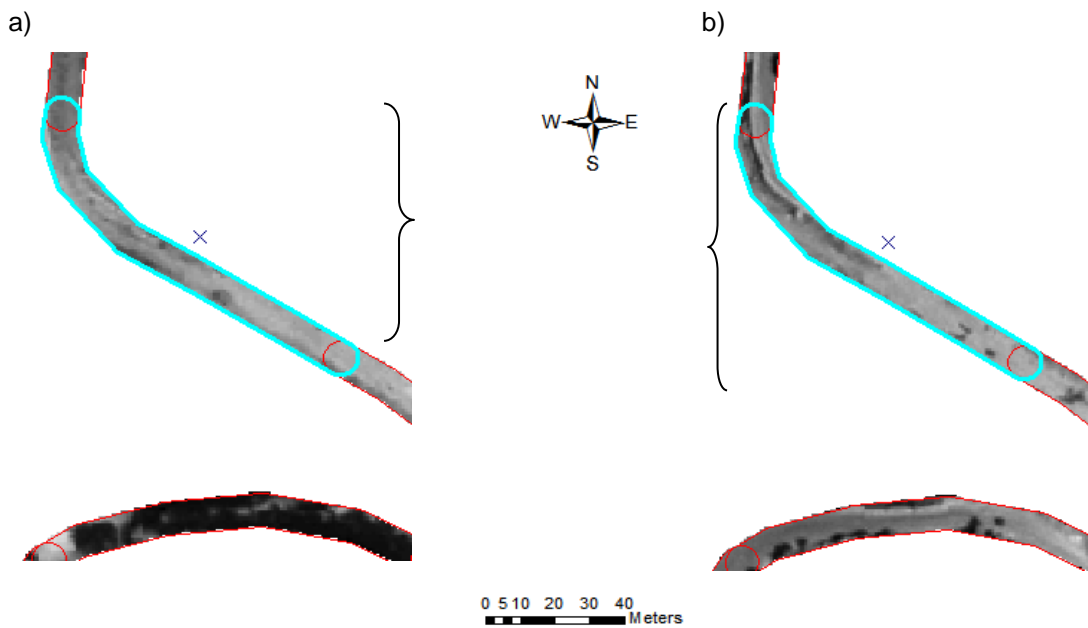
214

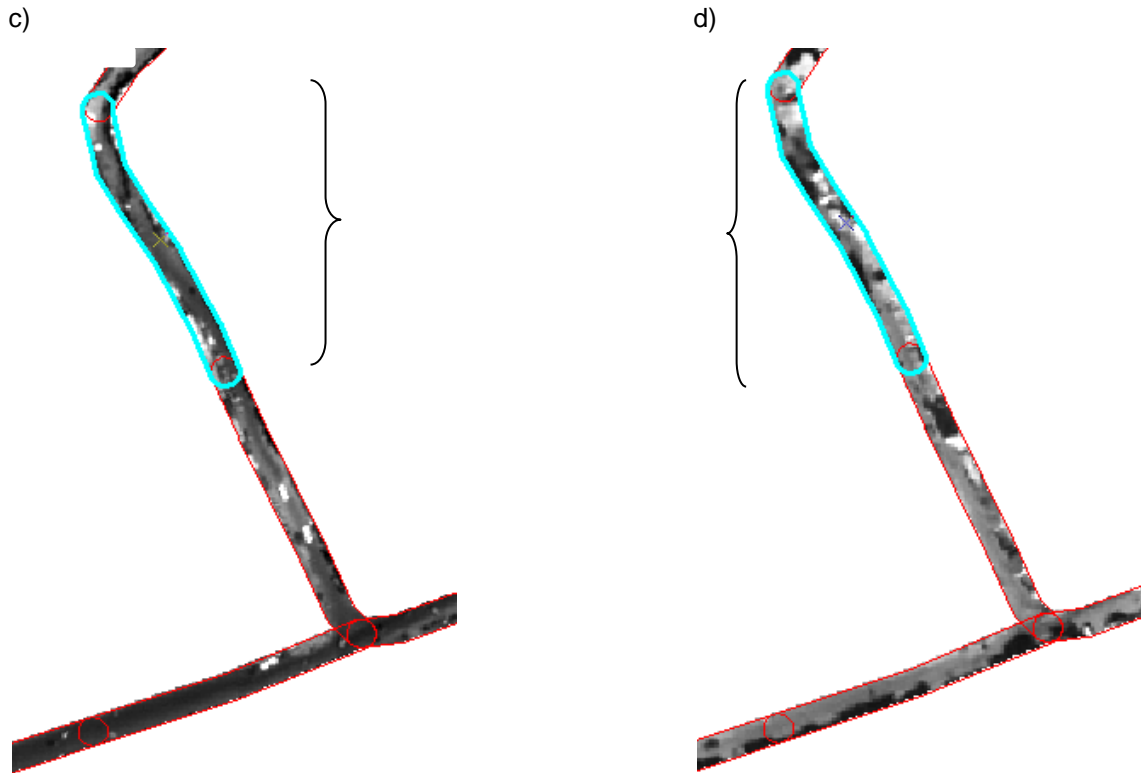
215

216

217

Figure 3: Workflow showing the enhanced change detection index (ECDI) for the roads in Muzaffarabad. The pre- and post-disaster images (outputs from the workflow shown in Figure 2) are normalized and a value pertaining to the roughness and edges are calculated for each road segment. The gradient is calculated for each road segment in each for the pre- and post-disaster images individually and then normalized (Equation 1). The change-related parameters for each road segment are then regressed with the visual index to find the coefficients to create the ECDI.





218 Figure 4 a) and b) are the pre- and post-images of the clipped roads. By looking at these images, a visual index of 2
 219 was determined and assigned because the roads have not changed much between the two images. C) and d) show a
 220 considerable change, hence a value of 9 is used as the visual index. Thirty road segments were visually analysed and
 221 an appropriate visual index determined in Muzzaffarabad.

222

223 2.3.4. Regression

224 The visual index derived by observing the visual changes in pre- and post-disaster images for 30 road
 225 segments was regressed with the values obtained from change in texture, gradient, and edges.

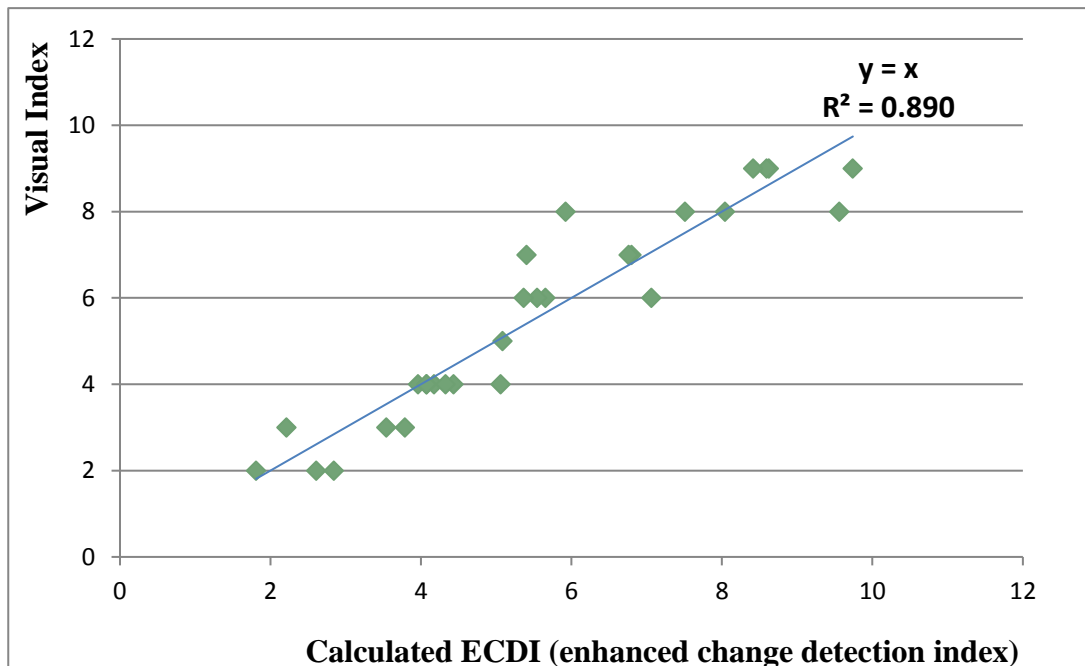
226

PAN_Texture	PAN_Gradient	PAN_Edges	IR_Texture	IR_Gr	Visual_Index
0.221810963	0.530726738	0.09235763	0.2175515	0.548	6
0.22992012	0.5103156	0.07699201	0.2006765	0.548	6
0.200479416	0.549637636	0.09600959	0.1956632	0.548	5
0.235774628	0.489457392	0.10375624	0.166315	0.518	4
0.152853313	0.550523211	0.11808296	0.1979714	0.528	4
0.208402731	0.508932503	0.09840798	0.2059248	0.558	

227 Figure 5 The calculated normalized texture, gradient and edge values derived for each road object for (R, G, IR) and
 228 PAN bands are regressed with the visual index obtained by observing the visual changes in pre- and post-disaster
 229 images for 1/10th of the road segments. The obtained regression coefficients are then used to calculate the ECDI
 230 (enhanced change detection index) for all the roads.

231 The R square value was 0.89 with low P values for PAN and PAN-sharpened IR bands derived
 232 gradient, texture, and edge parameter. This low P value with a high R square combination indicates
 233 that changes in the predictors (gradient, texture, and edge) are related to changes in the response

234 variable (visual index), thereby indicating that the model explains a great deal of the response
235 variability. Red and green band derived parameters did not contribute significantly. The graph of the
236 visual index vs. ECDI is shown in Figure 6.



237
238 **Figure 6: The visual index (using Figure 4) vs. the calculated ECDI (enhanced change detection index) (Figure 5) for**
239 **the selected roads. The figure shows a good correlation between the visual index and the pre- and post-disaster**
240 **normalized parameters (texture, edges, and gradient) used to create ECDI.**

241

242

243 **2.4. Open Spaces**

244 The open spaces were detected by segmenting the pre-disaster panchromatic sharpened green image
245 using a Meanshift segmentation algorithm (see the workflow in Figure 7). Camp sites mostly within
246 2km from the main roads and within areas 10,000 and 50,000 m² in Van and Muzaffarabad were
247 selected as probable camp-sites. Each selected polygon was used to clip the open space off the pre-
248 and post-event panchromatic and PAN (panchromatic)-sharpened images. The same rationale applied
249 in the accessibility workflow was used for open spaces. The workflow shown in

250 Figure 7 was used to detect local changes.



251

252 **Figure 7: Workflow for open spaces. Co-registered high-resolution pre-disaster images are segmented using the**
 253 **mean shift on the Green band to select homogeneous regions. Then an area threshold and a distance from the main**
 254 **roads are assigned to select the most suitable and accessible open spaces for campsites. The thresholds vary in the**
 255 **two case studies.**

256

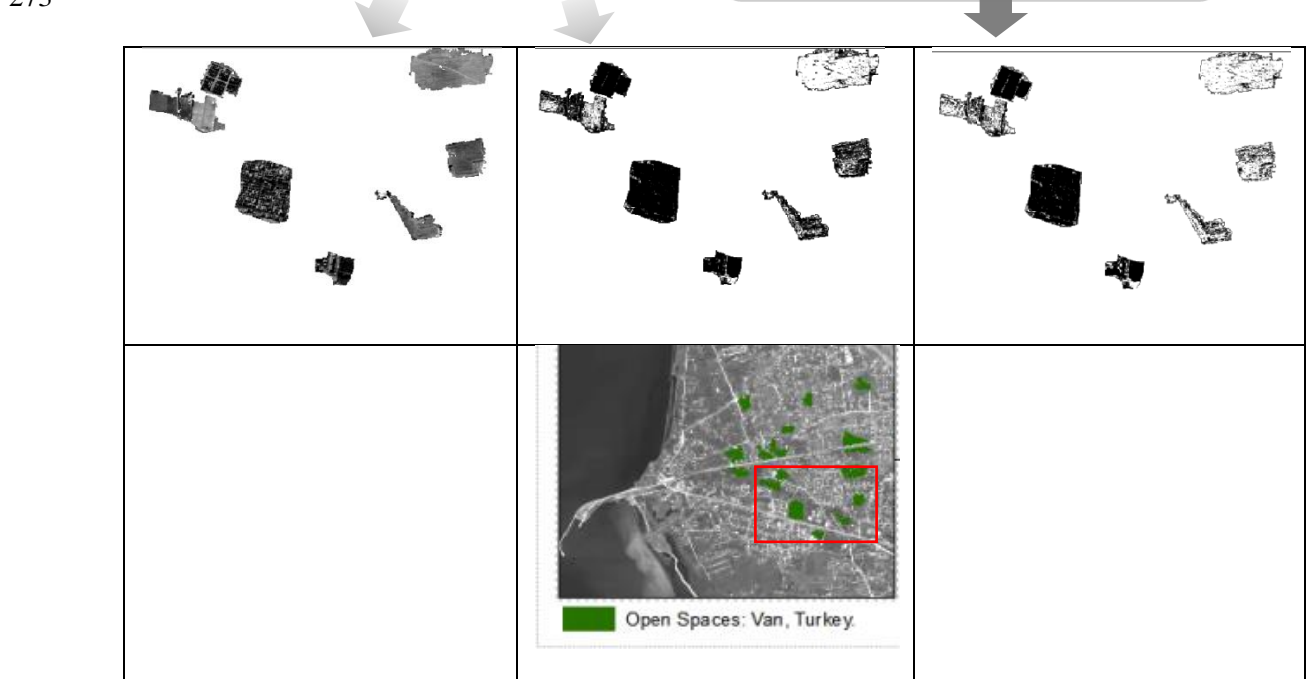
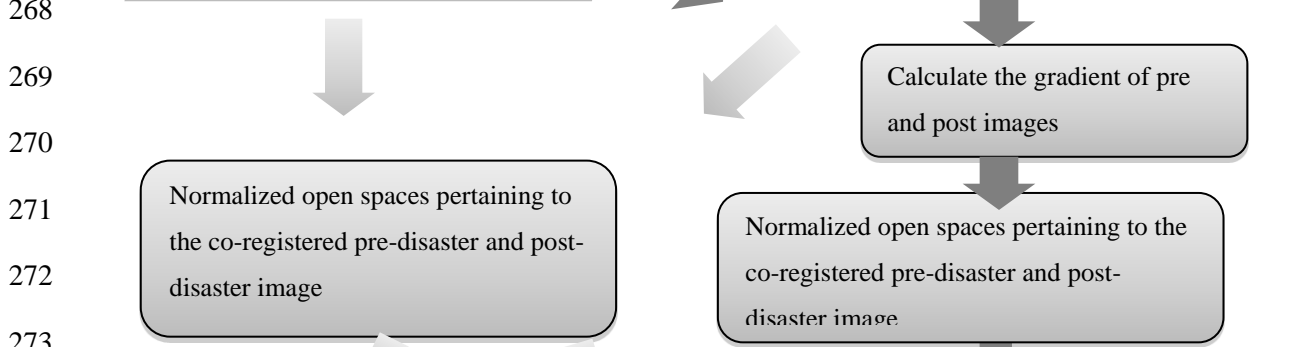
257 **2.4.1. Enhanced Change Detection Index (ECDI) for Open Spaces**

258 As shown in Figure 8 the ECDI for each open space was calculated similarly to the road segments by
 259 first obtaining the normalized difference between the PAN-sharpened, geo-referenced pre- and post-
 260 disaster images (bands PAN, and PAN-sharpened IR, Red, and Green) using Equation 1. Similar to
 261 the road segments, the images were subjected to a texture (roughness filter) and edge extraction
 262 (Vigra edge). Each open space area segment was assigned a number based on the texture/roughness
 263 and edge density in all bands. Then the gradient was calculated for each open space segment in the

264 pre- and post-disaster images. The gradients were then pre/post normalized using Equation 1 to obtain
 265 a value for each open space area.



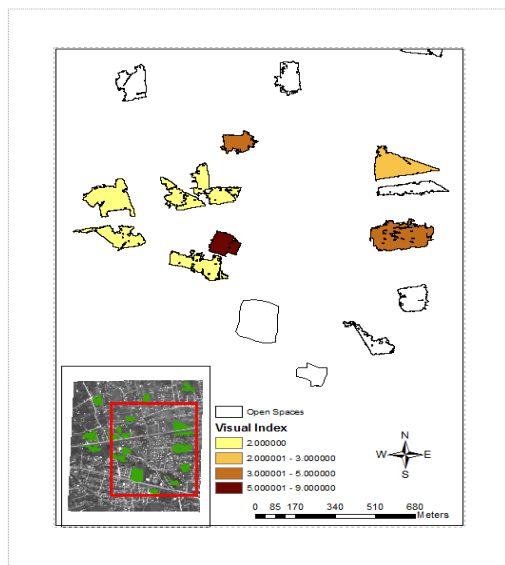
266 INPUT I: Open spaces of the co-registered pre-disaster image
 267 INPUT 2: Open Spaces of the co-registered post-disaster image



274 Index pertaining to the roughness of the normalized image
 275 Index pertaining to the edges of the normalized image
 276 Index pertaining to the gradient of texture of the normalized image

277

278



Regression of indices
with some visual indices
of the open spaces



OUTPUT: ECDI for each open
space shown in Figure 12

279

INPUT 3: Visual Index based on
INPUT 1 and INPUT 2 of randomly
selected open spaces

280

281

282 **Figure 8: The workflow of the change index for open spaces. The flowchart shows how the normalized images are**
 283 **calculated from the pre- and post-disaster images and the texture, gradient, and edge differences within each object,**
 284 **which are used to regress with the visual index of open spaces. The regression coefficients are used to calculate the**
 285 **enhanced change detection index (ECDI) for all the objects.**

286

287 2.4.2. Visual Index (Training Data) for Open Spaces

288 Similar to the road segments, for open spaces a visual index (VI) between 0 and 10 is developed by comparing the pre
 289 comparing the pre and post images visually in a way that is analogous to a linear visual scale to represent change. As
 290 represent change. As shown in

291 Figure 9, pre and post images for open spaces (objects) were used to determine the visual change. As for the road
 292 segments, the open spaces that had mild changes were assigned a small VI (close to 0,

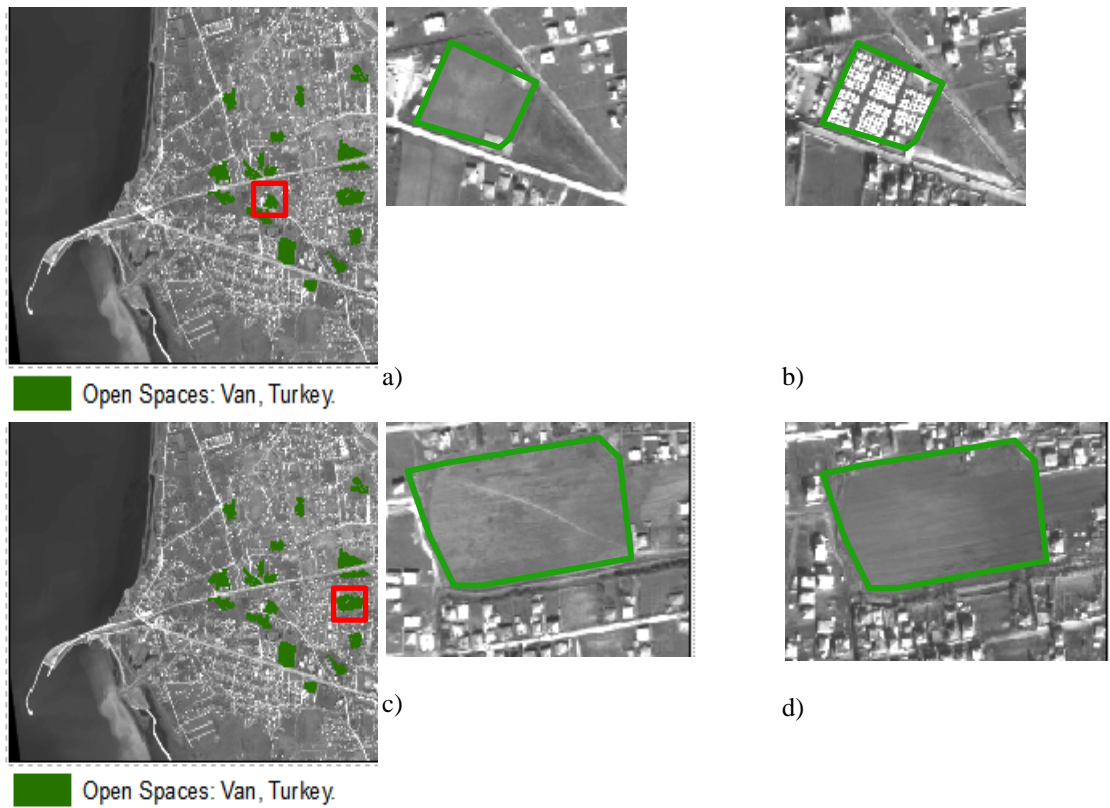
293 Figure 9 c) and d)) and the segments that showed large changes were assigned large VI values (close to 10,

294 Figure 9 a) and b)). Then as seen in Figure 8, this visual index was used as a training set and

295 regressed against the derived values of pre-post normalized gradient, edges, and roughness of each

296 open space.

297



298

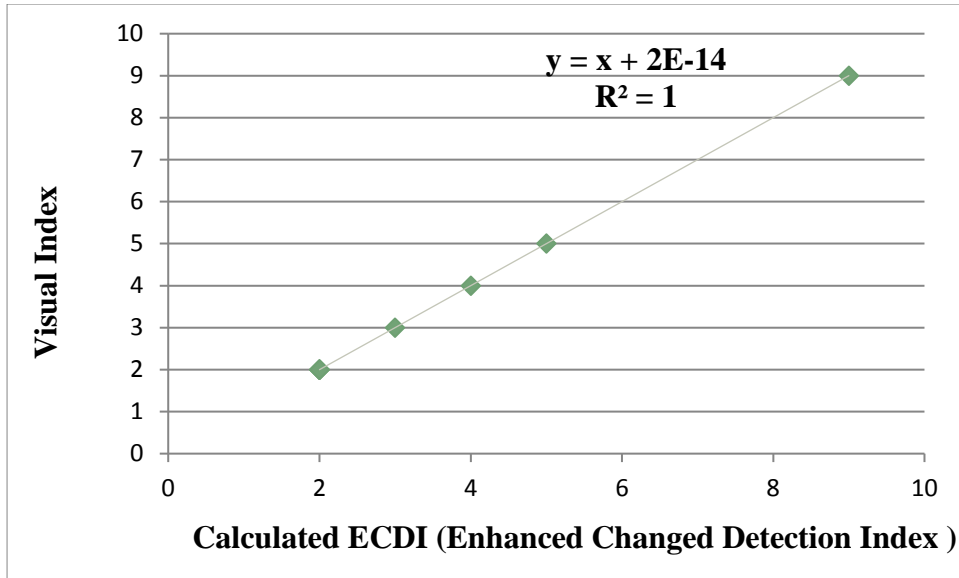
299 **Figure 9 a) and b) show the pre- and post-disaster images of an open space occupied as a campsite. C) and d) show**
 300 **the pre- and post-disaster images of an open space not occupied by a campsite after disaster. The visual differences**
 301 **between the open space are shown in a) and b) is large, so it is given a visual index of 9. The visual difference**
 302 **between the open space are shown in c) and d) is relatively small, hence is given a visual index of 3. A visual index smaller than**
 303 **3 was not given because there were significant differences in the grass patch between the pre- and post-disaster**
 304 **images.**

305

306 2.4.3. Regression

307 A methodology similar to that used for roads was utilized for open spaces. Through regression we
 308 acquired the coefficients needed to combine the derived pre-post normalized gradient, edge and
 309 roughness parameters with the visual perception (VI) to form an ECDI for all the open spaces,
 310 especially where the change were ambiguous to quantify visually. The R square value was 1 with low
 311 P values for gradient and edge parameters derived from PAN-sharpened IR band .The combination of
 312 a low P value with a high R square indicates that changes in the predictors (texture, edges, and
 313 gradient changes to the object) are related to changes in the response variable (visual index), so the
 314 model explains a great deal of the response variability (visual index). Unlike in roads, PAN-sharpened
 315 IR bands show dominance over the PAN for open spaces, particularly those covered in vegetation.
 316 Red and Green band derived parameters did not contribute significantly. The graph of visual index
 317 vs. ECDI is shown in Figure 10.

318



319

320 **Figure 10: The visual index (as seen in Figure 10) vs. calculated ECDI (**

321 **Figure 9) for the selected open spaces. The figure shows a good correlation between the visual index and the pre/post**
 322 **normalized changes in texture, edges, and gradient used to calculate the ECDI.**

323

324 **3. Results**

325 **3.1. Accessibility**

326 Figure 11 shows the pre/post normalized relative change (ECDI) for the road network in
 327 Muzaffarabad. The higher ECDI indicates a significant change, implying that the roads have changed
 328 since the disaster when compared to the pre-disaster image. Knowing if a road segment has changed
 329 relative to the other roads can allow emergency vehicles to find an alternative route that has very little
 330 change. Because remotely sensed data let us process large areas, alternative routes can be easily
 331 found.

332 As shown in

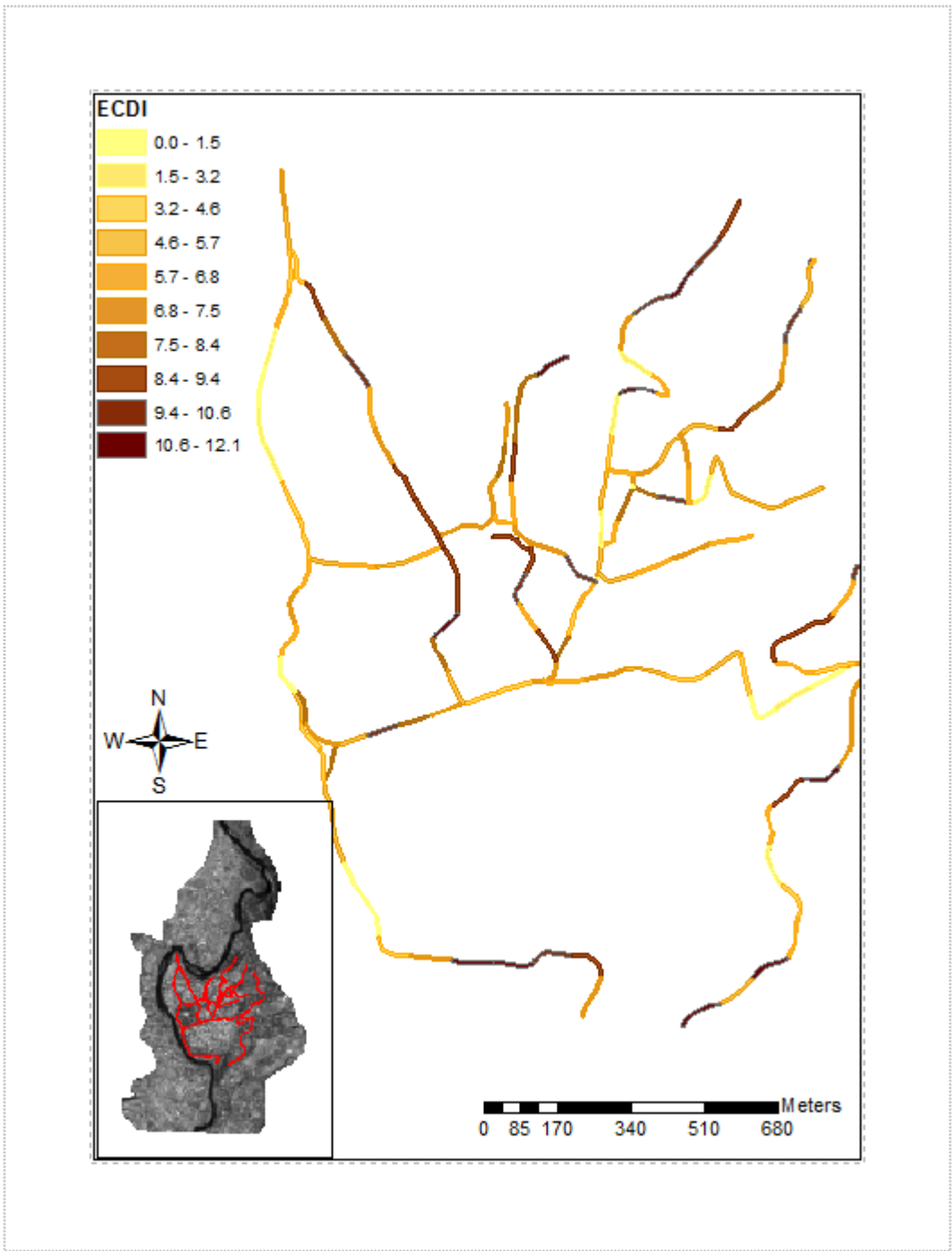
333

334

335

336

337 Table 3, each image can be compared to the pre-disaster image as well as an image immediately
 338 following a post-disaster image to get a better picture of the recovery situation.



339

340 **Figure 11: Enhanced change detection index (ECDI) for roads obtained between pre-disaster and post-disaster.**
 341 **Higher indices (represented by darker colors) indicate greater changes after disaster.**

342

343

344

345

346

347

348 **Table 3 Accessibility Case Study Scenarios**

349 Table 3 outlines scenarios that can be seen when ECDIs are observed over time. They are obtained by
 350 comparing post-disaster images to pre-disaster image.

ECDI of Pre disaster & Post T1*	ECDI of Pre disaster & Post T2*	ECDI of Post T1* & Post T2*	Scenario
>5	<5	>5	Road affected by post T1 date and recovered by Post T2 date
>5	>5	<5	Road affected by post T1 date and NOT recovered by Post T2 date
<5	<5	<5	Road not affected
<5	>5	>5	Road not affected by post T1 data and not modified by Post T2 date

351 *Post T1 and Post T2 are dates after the disaster.

352 As seen in

353

354

355

356

357 Table 3 the variation of roads affected by the disaster and recovered by the post T1 date and/or post
 358 T2 date can be determined. By obtaining the ECDI over time (

359

360

361

362

363 Table 3), the condition of roads over time can be used to improve management practices during future
 364 scenarios.

365

366 **3.2. Open Areas**

367 Shown in Figure 12 is the final output of the ECDI of open areas. The higher numbers in the ECDI
 368 indicate a major change in the open areas, probably due to the building of campsites after disaster. As

369 seen in Table 4, by obtaining the ECDI for the two post-disaster images and then comparing them to
 370 the pre-disaster image, we were able to identify open spaces that were turned into campsites, then
 371 back to open spaces by the post T2 date, as well as the open spaces that remained as campsites by the
 372 post T2 date. With more post-disaster images, a progressive recovery can be observed.

373 The return of open spaces to their original state is an indication of normalcy and hence an important
 374 aspect of recovery monitoring over time. Areas in which open spaces stay occupied by camps for a
 375 long period of time indicate slow resettlement and development efforts as compared to the areas in
 376 which the campsites are cleared up. The location, size and relative change of the open spaces over
 377 time can be used by managers to better understand management practices pertaining to re-housing of
 378 the population and development efforts.

379

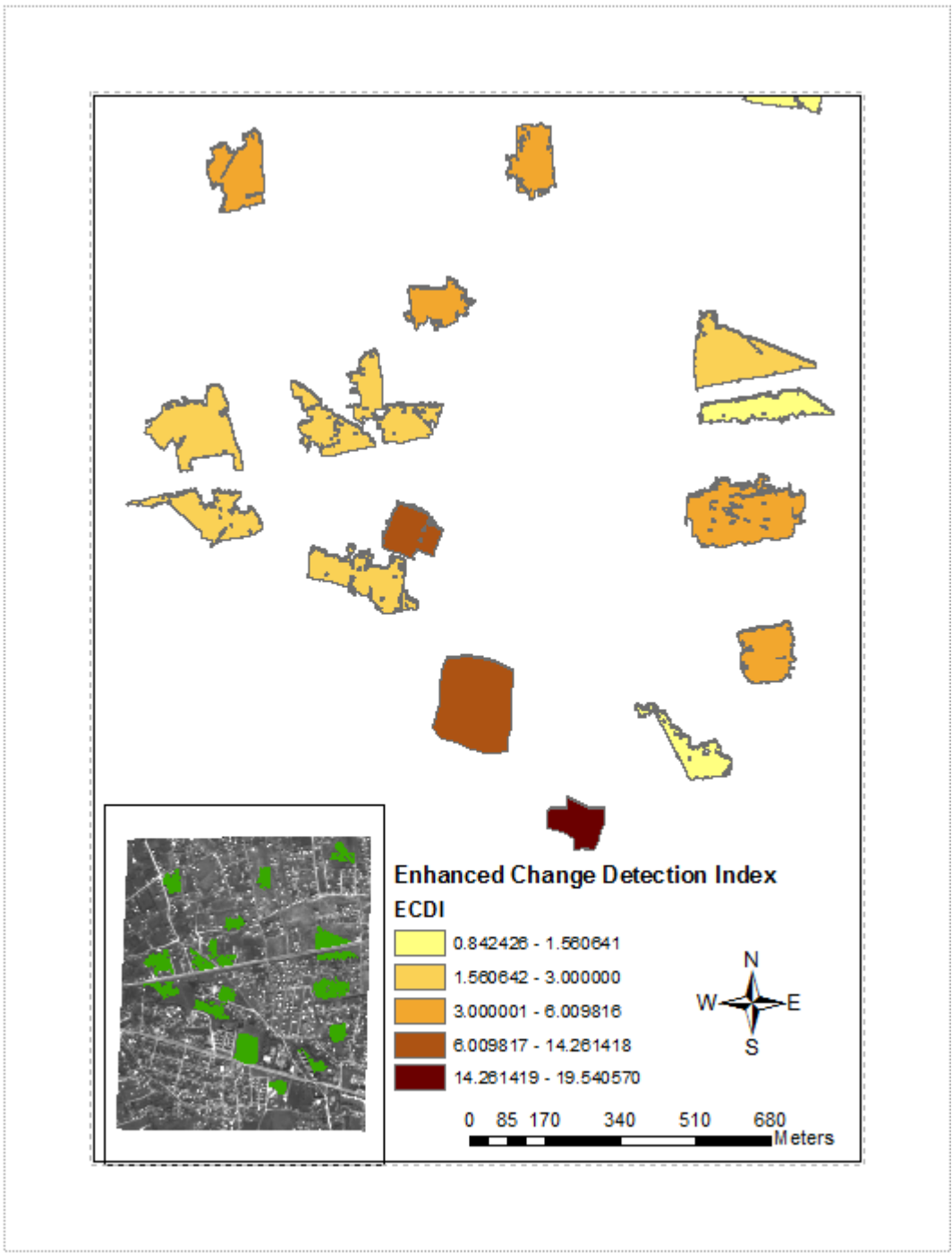
380 **Table 4 Open Spaces Case Study Scenarios**

381 This table notes scenarios that can be seen when enhanced change detection indices are observed over
 382 time.

ECDI of Pre disaster & Post T1*	ECDI of Pre disaster & Post T2*	ECDI of Post T1* & Post T2*	Scenario
>5	<5	>5	Open spaces occupied by camp site at Post T1* date and camp site removed by Post T2* date
>5	>5	<5	Open spaces occupied by camp site at Post T1* date and camp site still exists by Post T2* date
<5	<5	<5	Open spaces not occupied by camp sites
<5	>5	>5	Campsites not present at Post T1* date but campsites or development occurred at Post T2* date

383 *Post T1 and Post T2 are the dates that images were obtained after the disaster.

384



385

386 **Figure 12: ECDI for the open areas of Van. Higher indices (represented by darker colors) indicate larger changes**
 387 **after the disaster.**

388 **4. Discussion and Conclusions**

389 The proposed method uses indicators that pertain to recovery and monitoring as GIS objects and
 390 integrates existing knowledge into processing to optimize change detection. Each road class would
 391 have a specific texture, width, proximity to buildings, traffic, etc.; thus road types are compared with
 392 similar road types and bridges with similar bridges. In this study we separated primary roads from
 393 secondary roads. Provided one has more information about additional road categories, major and

394 minor roads within primary roads could be sub-categorized and analysed separately. This would also
395 discriminate roads with heavy traffic from roads with less traffic, roads surrounded by trees from
396 roads surrounded by buildings, and roads constructed of different materials, thereby increasing the
397 accuracy.

398 This method uses the calculation of the texture, edges, and gradient of each object to better estimate
399 the change between the pre- and post-disaster data. To determine what proportions of each of the
400 above properties contribute to real change, a visual index is used to train the data. Like any user-
401 derived parameter, the visual index can be very specific to the user. However, provided that the visual
402 index is completed by a single user, it should contain relative differences representative of the
403 changes within the image. It is easy to visually see objects that underwent a large change and those
404 that experienced no change, so more objects at extremes were used for the visual index. It is best to
405 use more objects at the ends of the change spectrum since the computer is then better able to estimate
406 objects that are at different gradients of change.

407 The normalization between the pre- and post-disaster data reduces the differences caused due to the
408 acquisition times and atmospheric anomalies of the pre/post images. The targeted change is relative to
409 all roads in a particular road group. Thus the normalization specifically enhances the relative change,
410 downplaying changes common to all roads in a particular road group. The VHR sensors used in this
411 study collect data around the same time, so the shadow effect due to acquisition time will be minimal;
412 the main issues are the incidence angle and changes in solar zenith, because these will impact the
413 imagery more directly than the difference between acquisition times. The considered relative change
414 by normalizing between the pre and post images would give more weight to the changes than the
415 increase and decrease in shadows. During a non-rush hour the main roads will still have more vehicles
416 than the alternative roads. Hence the vehicle changes due to the time of the day would not affect the
417 analysis as this is a relative change normalized to all roads.

418 After a disaster, as seen in Figure 4 d) rubble and trees fallen on the road can be factors that cause
419 change compared to the pre disaster image Figure 4 c). Rubble and fallen trees are brought out as a
420 change easily in the pre/post normalization, unless the texture of the rubble mimics the texture created
421 by vehicles in the same segment of the pre-disaster image. Most houses are not built close to
422 highways, so rubble that resembles highly dense vehicle traffic is unlikely to affect the analysis.
423 Rubble is primarily seen at the edges of the road and is visually different from the traffic seen in the
424 two case studies; hence it was flagged as a change in both cases.

425 Once the change is quantified based on training data, the pre/post normalized method outlined in this
426 paper can be used automatically to detect change and to observe recovery over time. Comparing the
427 most recent image and consecutive past images can give a complete history of changes pertaining to

428 road segments. Another benefit is that this method can be used over large areas to get the big picture
429 and determine changes over time.

430 The coefficients pertaining to the texture, edges, and gradient obtained from the visual index are
431 transferable to other roads with similar construction material and thus similar reflective properties.
432 This transferability works better for roads that are categorized to finer classes and are analysed
433 separately. The same method can be applied to other categories such as bridges and railroads when
434 analysed separately as a unique class of GIS objects. Buildings could also be analysed; this work has
435 been completed and will be published as a follow-up. Applying this method of analysis over time is a
436 significant advantage over analysis of ground truth data in temporal analysis. Analysis over time also
437 contributes to the full picture of the recovery and development after disaster, thereby giving managers
438 a tool to better understand management practices.

439

440 **Acknowledgements** This research was partly supported by the European Commission under FP7 (Seventh Framework
441 Programme): “SENSUM: Framework to Intergrade Space-based and in-situ sENSing for dynamic vUlnerability and recovery Monitoring”
442 (312972). We gratefully acknowledge the contribution from Enrica Verrucci and the anonymous referees.

443

444 References

- 445 Akcay, H.G., and S. Aksoy. 2008. 'Automatic Detection of Geospatial Objects Using
446 Multiple Hierarchical Segmentations'. *IEEE Trans. Geosci. Remote Sensing* 46 (7):
447 2097-2111. doi:10.1109/tgrs.2008.916644.
- 448 Al-Khudhairy, D.H.A., I. Caravaggi, and S. Giada. 2005. "Structural Damage Assessments
449 from Ikonos Data Using Change Detection, Object-Oriented Segmentation, And
450 Classification Techniques". *Photogrammetric Engineering & Remote Sensing* 71 (7):
451 825-837. doi:10.14358/pers.71.7.825.
- 452 Blaschke, T. 2010. "Object Based Image Analysis For Remote Sensing". *ISPRS Journal Of*
453 *Photogrammetry And Remote Sensing* 65 (1): 2-16. doi:10.1016/j.isprsjprs.2009.06.004.
- 454 Bouziani, Mourad, Kalifa Goita, and Dong-Chen He. 2010. 'Automatic Change Detection of
455 Buildings in Urban Environment from Very High Spatial Resolution Images Using
456 Existing Geodatabase and Prior Knowledge'. *ISPRS Journal of Photogrammetry And*
457 *Remote Sensing* 65 (1): 143-153. doi:10.1016/j.isprsjprs.2009.10.002.
- 458 Brown, D., Bevington, J., Platt, S., Saito, K., Adams, B. J., Chenvidyakarn, T., Spence, R. J.,
459 Chuenpagdee, R., Khan, A., So, E., (2012) “Monitoring and Evaluating Post-Disaster
460 Recovery Using High-Resolution Satellite Imagery – Towards Standardised Indicators

461 for Post-Disaster Recovery”, ReBuildDD Workshop, Cambridge, UK.

462 Butenuth, Matthias, and Christian Heipke. 2010. 'Network Snakes: Graph-Based Object
463 Delineation with Active Contour Models'. *Machine Vision and Applications* 23 (1): 91-
464 109. doi:10.1007/s00138-010-0294-8.

465 Dai, X and S. Khorram. 1998. 'The Effects of Image Misregistration on the Accuracy of
466 Remotely Sensed Change Detection'. *IEEE Trans. Geosci. Remote Sensing* 36 (5): 1566-
467 1577. doi:10.1109/36.718860.

468 Dell'Acqua F, Lisini G, Gamba P 2009. 'Experiences in Optical and SAR Imagery
469 Analysis for Damage Assessment in the Wuhan, May 2008 Earthquake'. *In:*
470 *Proceedings of IGARSS 2009, Cape Town, South Africa, 13–17 July 2009.*

471 Download.geofabrik.de.,2015. <http://download.geofabrik.de/europe/turkey.html>.

472 Earthquake.usgs.gov,. 2005. 'PAKISTAN'.
473 <http://earthquake.usgs.gov/earthquakes/eqinthenews/2005/usdyae/#details>.

474 Earthquake.usgs.gov,. 2011. 'EASTERN TURKEY: Van'.
475 <http://earthquake.usgs.gov/earthquakes/eqinthenews/2011/usb0006bqc/>.

476 Gueguen L, Soille P, Pesaresi M (2011) 'Change Detection based on Information Measure.'
477 *IEEE Trans Geosci Remote Sens* 49(11):4503–4515

478 Kodge, B. G., Hiremath, P. S. (2011) 'Automatic Open Space Area Extraction and Change
479 Detection from High Resolution Urban Satellite Images. CoRR abs/1103.4913 (2011)

480 Lin, Chungan, and Ramakant Nevatia. 1998. 'Building Detection and Description from a
481 Single Intensity Image'. *Computer Vision And Image Understanding* 72 (2): 101-121.
482 doi:10.1006/cviu.1998.0724.

483 Mena, J.B., and J.A. Malpica. 2005. 'An Automatic Method for Road Extraction in Rural and
484 Semi-Urban Areas Starting from High Resolution Satellite Imagery'. *Pattern
485 Recognition Letters* 26 (9): 1201-1220. doi:10.1016/j.patrec.2004.11.005.

486 Michaelsen, Eckart, Uwe Soergel, and Ulrich Thoennessen. 2006. 'Perceptual Grouping for
487 Automatic Detection of Man-Made Structures in High-Resolution SAR Data'. *Pattern
488 Recognition Letters* 27 (4): 218-225. doi:10.1016/j.patrec.2005.08.002.

489 Mohammadzadeh, A., M. J. ValadanZoej, and A. Tavakoli. 2009. 'Automatic Main Road
490 Extraction from High Resolution Satellite Imageries by Means of Particle Swarm
491 Optimization Applied to a Fuzzy-Based Mean Calculation Approach'. *Journal of the
492 Indian Society of Remote Sensing* 37 (2): 173-184. doi:10.1007/s12524-009-0021-y.

493 Mohammadzadeh, A., M.J. ValadanZoej, and A. Tavakoli. 2008. 'Automatic Main Road

494 Extraction from High Resolution Satellite Imageries by Means of Self-Learning Fuzzy-
495 GA Algorithm'. *Journal of Applied Sciences* 8 (19): 3431-3438.
496 doi:10.3923/jas.2008.3431.3438.

497 Pagot, E., M. Pesaresi, D. Buda, and D. Ehrlich. 2008. 'Development of an Object-oriented
498 Classification Model Using Very High Resolution Satellite Imagery for Monitoring
499 Diamond Mining Activity'. *International Journal of Remote Sensing* 29 (2): 499-512.
500 doi:10.1080/01431160601047771.

501 QGIS Development Team, 2015. QGIS Geographic Information System Developers Manual.
502 Open Source Geospatial Foundation Project. Electronic document:
503 http://www.qgis.org/wiki/Developers_Manual

504 Singh, P. P., and R. D. Garg. 2014. 'Road Detection from Remote Sensing Images Using
505 Impervious Surface Characteristics: Review and Implication'. *Int. Arch. Photogramm.
506 Remote Sens. Spatial Inf. Sci.* XL-8: 955-959. doi:10.5194/isprsarchives-xl-8-955-2014.

507 Talib, Muhamad Lazim, and SuzaimahRamli. 2015. 'A Review of Multiple Edge Detection in
508 Road Lane Detection Using Improved Hough Transform'. *AMR* 1125: 541-545.
509 doi:10.4028/www.scientific.net/amr.1125.541.

510 Touya, Guillaume. 2010. 'A Road Network Selection Process Based on Data Enrichment And
511 Structure Detection'. *Transactions In GIS* 14 (5): 595-614. doi:10.1111/j.1467-
512 9671.2010.01215.x.

513 VictorDevadoss, A., and S.M.A. Shahul Hameed. 2015. 'Analyzing the Behavioral Changes
514 of Road User through Euclidean Distance Intuitionistic Fuzzy Valued Associative
515 Memories'. *International Journal of Computer Applications* 118 (10): 23-27.
516 doi:10.5120/20782-3416.

517 Vu, T. T., and Y. Ban. 2010. 'Context-Based Mapping of Damaged Buildings from High-
518 Resolution Optical Satellite Images'. *International Journal of Remote Sensing* 31 (13):
519 3411-3425. doi:10.1080/01431161003727697.

520 Walter, Volker. 2004. 'Object-Based Classification of Remote Sensing Data for Change
521 Detection'. *ISPRS Journal Of Photogrammetry And Remote Sensing* 58 (3-4): 225-238.
522 doi:10.1016/j.isprsjprs.2003.09.007.

523 Yang, J., and R. S. Wang. 2007. 'Classified Road Detection from Satellite Images Based on
524 Perceptual Organization'. *International Journal of Remote Sensing* 28 (20): 4653-4669.
525 doi:10.1080/01431160701250382.

526